Core Flooding Experiments and Reactive Transport Modeling of Seasonal Heat Storage in the Hot Deep Gassum Sandstone Formation

Holmslykke, Hanne D.; Kjøller, Claus; Fabricius, Ida Lykke

Published in:
ACS Earth and Space Chemistry

Link to article, DOI:
10.1021/acsearthspacechem.7600031

Publication date:
2017

Document Version
Peer reviewed version

Core flooding experiments and reactive transport modelling of seasonal heat storage in the hot deep Gassum Sandstone Formation

Hanne D. Holmslykke[a], Claus Kjøller[b] and Ida L. Fabricius[c]*

[a]Department of Reservoir Geology, Geological Survey of Denmark and Greenland, Øster Voldgade 10 DK-1350 Copenhagen K, Denmark

[b]Department of Geochemistry, Geological Survey of Denmark and Greenland, Øster Voldgade 10 DK-1350 Copenhagen K, Denmark

[c]Department of Civil Engineering, Technical University of Denmark, Brovej 118, DK-2800 Kgs Lyngby, Denmark

KEYWORDS High temperature aquifer thermal energy storage, Deep aquifer thermal energy storage, Reactive transport modelling, Flooding experiments, Gassum Formation

ABSTRACT

Seasonal storage of excess heat in hot deep aquifers is considered to optimise the usage of commonly available energy sources. The chemical effects of heating the Gassum Sandstone Formation to up to 150°C is investigated by combining laboratory core flooding experiments with petrographic analysis and geochemical modelling. Synthetic formation water is injected into two sets of Gassum Formation samples at 25°C, 50°C (reservoir temperature), 100°C and 150°C with a velocity of 0.05 PV/hr and 0.1 PV/hr, respectively. Results show a significant increase in the aqueous concentration of silicium and iron with increasing temperature due to dissolution of silica and siderite. Increasing the reservoir temperature from 50°C to 100°C enhanced the naturally occurring weathering of Na-rich feldspar to kaolinite. Dissolution of quartz increased sharply above 100°C and was the dominating process at 150°C, resulting in a significant increase in the aqueous silicium concentration. At temperatures ≤100°C, the silicium concentration was controlled by a quasi-stationary state between feldspar dissolution and kaolinite precipitation while the concentration was kinetically controlled by quartz dissolution at 150°C. Furthermore, a strong coupling between dissolution, precipitation and flow velocity was observed.

The results of this study show that the effects of heat storage of up to 150°C in the Gassum Formation in the Stenlille area is expected to have only minor effects on the properties of the reservoir and that storage of excess heat in the Gassum Formation in the Stenlille area may be possible provided operational precautions are taken.

1. INTRODUCTION

A temporal mismatch typically exists between the supply and the demand for heat. For example, during the summer excess heat is produced from waste incineration, while the demand for energy peaks during the winter. Seasonal storage of surplus heat in the subsurface may overcome this incongruity between supply and demand for heat. During summer, formation water is extracted from the aquifer and heated using the available surplus energy prior to reinjection into the reservoir. During winter, the stored hot water is extracted and used for district heating.

In Denmark, geothermal energy for district heating is already being extracted from deep sandstone aquifers with temperatures up to 75°C[1]. Consequently, the possibility of seasonally storing excess heat in these geothermal aquifers is considered. Due to a relatively high *in situ* temperature combined with a low aquifer flow rate, the heat loss may be minimised in these aquifers. Furthermore, the heat storage may increase the heat potential in the aquifers and possibly prolong the life time of the geothermal aquifer[2, 3].

Heat storage in geothermal aquifers will inevitable increase the temperature of the aquifer. Temperature is known to exert an important control on both the extent and rate of reactions of minerals in the aquifer. Generally, elevated temperatures increase reaction rates, while mineral solubility can either increase or decrease, depending on the thermodynamic properties of the mineral[4-9]. For example, increasing the temperature leads to higher solubility of silicates, but lower solubility of carbonates. The exponential dependence of reaction rates on temperature implies that the effects of the temperature becomes more pronounced at higher temperature differences[4, 10]. Dissolution/precipitation processes in the aquifer may affect the permeability of the aquifer by changing the pore space geometry and pore connectivity[11-13]. Furthermore, dissolution of the cementing material in the aquifer may reduce the mechanical strength of the

aquifer. A major concern is therefore that heat storage may permanently damage the aquifer making extraction of further geothermal energy unfeasible.

Aquifer thermal energy storage systems in shallow aquifers injecting water with a temperature of up to approximately 20°C and small temperature differences ($\Delta T < 15°C$) are operating successfully in many countries[3, 14, 15]. Experiences with higher operational temperatures (up to 150°C) are less frequently reported[6, 7, 16, 17]. Laboratory[18-22] and field[7, 16] tests show that the release of silicium increases sharply at elevated temperatures due to the dissolution of quartz and feldspars, while precipitation of several secondary minerals, including kaolinite, boehmite, gibbsite, montmorillonite has been observed. Field tests of heat storage in confined shallow sandstone aquifers at temperatures up to 150°C[7, 16] revealed, however, calcium carbonate precipitation as the critical water chemistry problem. Softening of the water before heating was necessary to prevent scaling in the heat exchanger and storage well for successful operation of the heat storage. A deep aquifer thermal energy storage system injecting surplus heat at a depth of approximately 1200 m at a temperature of 90°C is operating successfully in Neubrandenburg, Germany[17].

Though the chemical reactions that potentially occur when heated formation water is injected into the aquifer to a large extent is known, the rate, extent and coupling of these reactions are highly site specific. In this study the potential geochemical reactions due to heat storage of up to 150°C in the deep subsurface of Denmark is investigated. Core flooding experiments combined with petrographic analysis and geochemical modelling is conducted to identify the primary chemical reactions that potentially occur when heated formation water is injected into the aquifer. As a case study the Upper Triassic – Lower Jurassic Gassum Formation in the Stenlille area is used because the Gassum Formation is the most widespread geothermal aquifer in

Denmark. As calcite cement is extremely rare in the Gassum Formation in the Stenlille area, heat storage in this area may be viable since the operational problems caused by precipitation of calcite upon cooling of the formation water may be avoided or at least minimised.

2. MATERIALS AND METHODS

2.1. Geological background. The Gassum Formation is present in most of the Danish area (Figure 1) at a burial depth of 850 to 3350 m and is one of the most abundant Danish geothermal reservoirs. The deposition initiated during the Upper Triassic 209 mio years ago and continued during a series of relative sea level falls[23]. Thus, the Gassum Formation consists of several regressive shoreface and fluvial sandstones of wide lateral extent interbedded with mudstones deposited in either marine, lagoonal and lacustrine environments[23]. The thickness of the Gassum Formation varies from 50 – 150 m in the Danish area, though thicknesses up to 300 m occur locally due to salt structures and major faults[23, 24]. The Gassum Formation forms an anticlinal structure with a vertical closure of 35 m covering an area of 14 km^2 in the Stenlille area[25]. The individual reservoir intervals of well to moderately sorted, fine to medium-grained sandstone are typically 10 m thick in the Stenlille area, though may be up to 60 m thick beneath the structural closure.

The Gassum Formation is directly overlain by thick (up to 1000 m) marine mudstones of the Lower Jurassic Fjerritslev Formation with large lateral continuity in the Danish part of the Norwegian–Danish Basin, a thinner (few hundred metres) Middle Jurassic – Lower Cretaceous succession and a thick (up to 2000 m) Upper Cretaceous chalk/limestone succession[23, 26]. The Gassum Formation overlies the restricted marine mudstones of the Upper Triassic Vinding Formation and is covered by the marine mudstones of the Lower Jurassic Fjerritslev Formation.

The sandstones of the Gassum Formation are mainly subarkoses and arkoses[27] according to the classification by McBride (1963)[28]. The quartz content is highest in sandstones from the Stenlille area, whereas cored intervals from Jutlandic wells show higher contents of feldspar and rock fragments. The Gassum Formation at the Stenlille area has a very mature mineralogical composition and calcite cement is extremely rare. Organic matter is typically not observed in samples from the Stenlille area, although one sample showed an organic matter content of 6%.

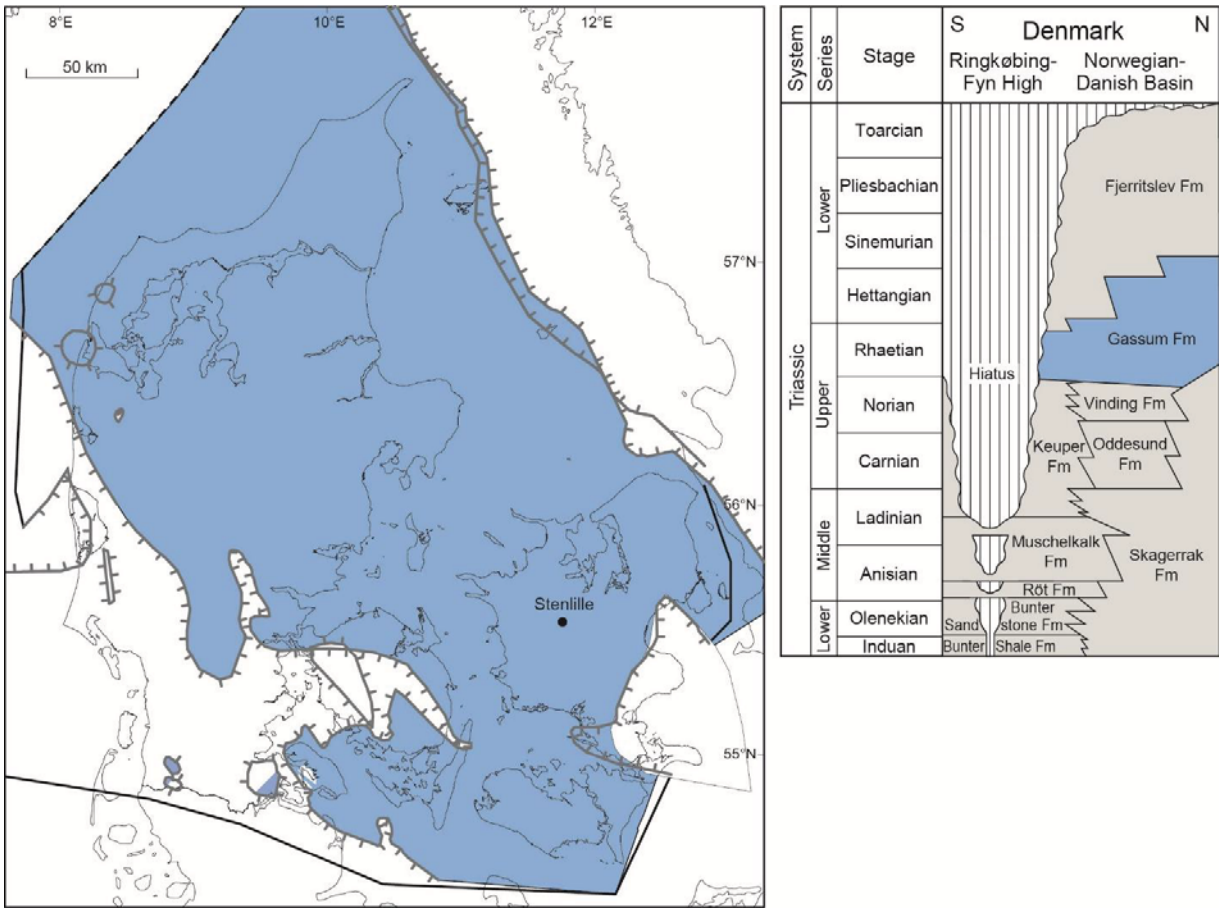

Figure 1. Map of Denmark showing the extent of the Gassum Formation in blue colour (to the left) and the stratigraphic scheme (to the right). Modified from[29]

2.2. Sample description and fluid. In order to represent one of the most abundant Danish geothermal reservoirs, two cylindrical specimens ($S_{0.05}$ and $S_{0.1}$) were prepared from a cored interval of the Upper Triassic – Lower Jurassic Gassum Formation in the Stenlille-2 well (Figure 1). The tested samples had the approximate length and diameter of 74.5 mm and 38.0 mm, respectively, and were selected from the same depth in the core (1539.50 m) to ensure close similarity. The temperature of the reservoir is approximately 50°C, and the porosity (Φ), gas permeability (K_g) and Klinkenberg permeability (K_L) of the two samples prior to testing were $\Phi_{S0.05}$ = 29.11%, $K_{g,S0.05}$ = 195 mD, $K_{L,S0.05}$ = 183 mD and $\Phi_{S0.1}$ = 28.85%, $K_{g,S0.1}$ = 181 mD, and $K_{L,S0.1}$ = 177 mD, respectively.

QEMSCAN® analysis of two samples from the same depth (1539.0 m) as the tested samples show that the Gassum Formation primarily consists of quartz (72 % of solid) and secondarily of feldspar (8% K-feldspar and 2.5% Na-feldspar) with minor contributions from kaolinite, mica, siderite and heavy minerals. The QEMSCAN® analysis is thus in line with previous observations of the mineralogy of the Gassum Formation[30].

Table 1. Chemical composition of the synthetic Gassum brine used in the experiments in this study. The brine has been modified from[31].

	Concentration (mg/L)
Na	59,000
K	1,100
Mg	1,600
Ca	11,500
Sr	660
Cl	116,329
HCO_3^-	80
SO_4^{2-}	30

The chemical composition of the Gassum flooding brine is modified from Laier (2008)[31] and is shown in Table 1. The brine salinity is 17.02% with sodium and chloride being the dominating ions while calcium, magnesium and potassium also are present in significant amounts. The silicium and aluminium concentrations were not measured by Laier (2008)[31]. Initial chemical speciation calculations with PHREEQC[32] using the Pitzer and the Thermodem[33] databases show in both cases that the Gassum brine is subsaturated with respect to sulphates such as anhydrite and celestine and to carbonates such as calcite and dolomite at all temperatures applied in the experiments.

2.3. Experimental procedure. In all, two core flooding experiments were performed such that one experiment was performed with each of the two specimens from the Gassum Formation. Synthetic Gassum brine was used as the flooding fluid, and flow velocities of 0.05 PV/hr (0.014 cm/hr) and 0.1 PV/hr (0.029 cm/hr) were applied for specimens $S_{0.05}$ and $S_{0.1}$, respectively. Prior

to testing, the specimens were cleaned in methanol to remove any salts precipitated from pore water. He-porosity, N_2-gas permeability and Klinkenberg permeability were measured prior to and after testing[34]. Mineralogical changes in the specimens were identified by thin section analyses using optical microscope and backscatter electron microscopy prior to and after the flooding experiments to identify major chemical reactions responsible for the observed changes in aqueous chemistry. The mineralogical observations provide information for the geochemical modelling. Prior to testing, the specimens were vacuum (at -1 mbar) and pressure (at 110 bar for three days) saturated in degassed formation water and the saturation state of the specimens was verified using the Archimedes test.

The experimental set up is illustrated in Figure 2. The brine saturated specimen was placed in a Viton sleeve inside a hydrostatic core holder and a confining pressure of 275 bar corresponding to the *in situ* pressure was applied. *In situ* pore pressure was assured by impressing a back pressure of 170 bar. A constant flow rate of either 0.05 PV/hr or 0.1 PV/hr was assured by high precision Quizix® pumps in two parallel experiments in the same oven. For both flow rates, tests were performed at 23°C, 50°C (reservoir temperature), 100°C and 150°C allowing flow for minimum one week at each temperature. Downstream the core holder, each of the flow lines was equipped with two sampling loops to collect effluent brine for chemical analysis. During sampling, flow was allowed to pass through one of the two loops. When sampling, the flow was shifted to the empty loop, and the loop with brine was dismantled from the oven and cooled fast to ambient temperature (23±1°C) before transferring the content of the loop to a syringe. Sampling from both flowlines (0.05 PV/hr and 0.1 PV/hr) was performed concomitantly in order to minimize temperature oscillation in the oven. After sampling, the loop was filled with distilled water, placed in the oven again and re-pressurised to 170 bar by injection of distilled water.

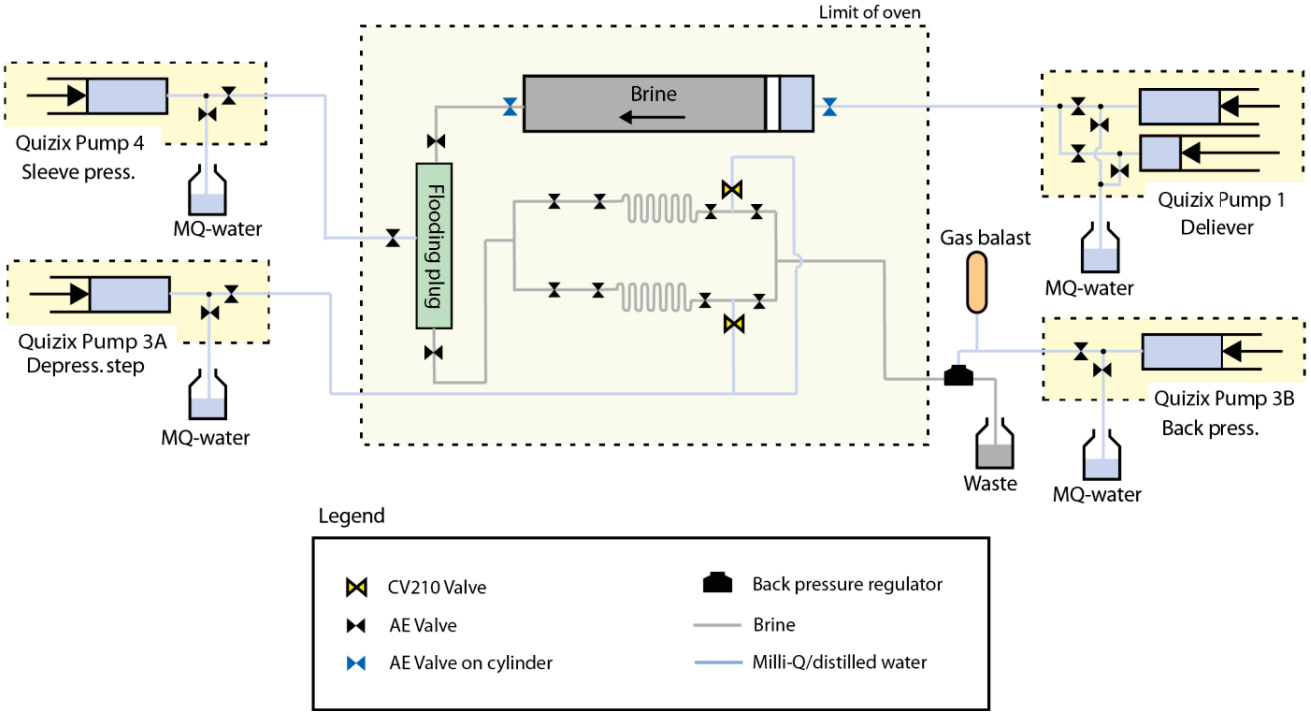

Figure 2. Experimental set up

The alkalinity and pH were measured immediately after sampling on unfiltered samples. The alkalinity was determined by Gran-titration[35]. The rest of the sample was passed through 0.22 µm cellulose-acetate syringe filter into three separate polyethylene vials. Samples for cation and silicium analysis received 1 vol% of 7M HNO_3 and 10 vol% of 5M NaOH, respectively, and was kept refrigerated until ICP-MS analysis (PerkinElmer Elan6100DRC Quadrupol) with a standard deviation of 3-15% depending on the element measured. Samples for anion analysis (chloride and sulphate) were frozen until ion-chromatography analysis (LC50-CD50, Dionex, CA, USA) with a quantification limit of 0.05 mg/L.

2.2 Reactive transport modelling. The injection of heated formation water into the Gassum Formation was modelled using the 1D reactive transport code PHREEQC version 3.0[32]. Combined with the petrographic analysis, the hydrogeochemical modelling helps identify which

minerals may possibly dissolve and/or precipitate when heated Gassum brine is injected into the Gassum Formation. A 1D transport model column, comprising 10 cells with a length of 0.0745 m each, was constructed and flushed with synthetic Gassum brine (Table 1) at 23°C, 50°C 100°C and 150°C and at 170 bar pressure. Dispersion was not taken into account in the model. The thermodynamic data from the Thermoddem database were used since this database is optimised to high temperatures and includes a large range of silica minerals. The Thermoddem database uses the Debye-Hückel theory[36] to calculate the activity coefficients of the ions in solution; an approach that is only valid for dilute solutions. For solutions of higher salinity, such as the Gassum brine, the Pitzer approach[37, 38] to define activities based on specific ion interactions is sometimes more appropriate. However, the Pitzer database only includes a limited range of aqueous species and minerals, excluding many of the minerals relevant for this study.

The model included the thermo-kinetic processes of mineral dissolution/precipitation reaction using the kinetic rate law given by[4, 10]:

$$R = k \cdot \frac{A_0}{V} \cdot \left(\frac{m}{m_0}\right)^{0.67} \cdot (1 - \Theta) \quad (1)$$

where R is the dissolution/precipitation rate (mol/L/sec), k the overall rate constant (mol/m^2/sec), A_0 the initial surface area (m^2), V the liquid volume (L), m the remaining mass of mineral, m_o the initial mass and θ the mineral saturation ratio given by θ = IAP/K, where IAP is the ionic activity product and K the equilibrium constant. The term $(m/m_0)^{0.67}$ corrects for changes in reactive surface sites during the dissolution/precipitation process[4].

The overall rate equation is a sum of multiple mechanisms of which those in pure water (neutral), and those catalysed by H^+ (acid) and OH^- (base) are included in the rate expression. The

dependency of the rate with temperature is calculated by the Arrhenius equation and the overall rate constant is given by[10]:

$$k = k_{25}^{N} exp\left[\frac{-Ea^{N}}{R}\left(\frac{1}{T} - \frac{1}{298.15}\right)\right] + k_{25}^{A} exp\left[\frac{-Ea^{A}}{R}\left(\frac{1}{T} - \frac{1}{298.15}\right)\right] a_{H}^{n_A} + k_{25}^{B} exp\left[\frac{-Ea^{B}}{R}\left(\frac{1}{T} - \frac{1}{298.15}\right)\right] a_{H}^{n_B} \quad (2)$$

where E_a is the activation energy (J/mol), k_{25} the rate constant at 25°C, R the gas constant (J/mol/K), T the temperature (K), and a_H the activity of H^+. The indices N, A and B refer to neutral, acid and base mechanisms, respectively. For most minerals, precipitation rate data are not available. Therefore, it is assumed that the same kinetic expression can be used for both dissolution and precipitation processes[39]. The initial amount of the minerals was calculated from the mineral content found by the QEMSCAN® analysis and rate constants and the initial specific surface area of the minerals were found in the literature[39, 40]. The specific reactive surface area is difficult to measure or calculate since only part of the mineral surface is involved in the reaction[19, 39]. For example, the hydrolysis of silicates has been shown only to occur at specific sites on the surface of reactant minerals[19, 41-43] . Therefore, the specific surface area was used to fit the model to the observed data. The geochemical model was fitted to the experimental data from the 0.1 PV/hr experiments and subsequently tested against the results of the 0.05 PV/hr experiment.

3. RESULTS AND DISCUSSION

3.1. Water chemistry. The effects of an increasing temperature on the aqueous concentration of selected parameters in the effluent are shown in Figure 3. Upon temperature increase, a clear and immediate increase in the aqueous silicium concentration is observed indicating dissolution of silicium bearing minerals. At each temperature, a constant level of silicium in the effluent is observed, the only exception being at 150°C where the silicium concentration does not seem to

reach steady state, especially at a flow rate of 0.05 PV/hr. The plateau reached at each temperature is identical for the two experiments, irrespective of the flow velocity, except at 150°C where a lower silicium concentration is measured for the slower flow rate.

The iron concentration generally peaks immediately after an increase in the temperature followed by a decreasing iron concentration. As observed for the silicium concentration, the measured iron concentration is lower at 150°C for the lower flow rate as compared to the higher flow rate. Test with the ferrozine method showed that the iron is present as Fe(II) indicating no or only limited intrusion of oxygen to the samples.

No observable changes were identified for the concentration of chloride, sulphate, potassium, calcium, magnesium and sodium, probably due to the very high content of these elements in the synthetic brine and the relative small changes that any reaction would cause. Aluminium remains below detection limit (0.03 mg/L) throughout the experiments (data not shown). The measured pH is relatively constant between 5 and 6 at all temperatures. An accurate pH measurement was difficult to obtain, since the pH drifted considerably during measurement. As a consequence both the pH measured immediately after sampling and the pH at the beginning of the alkalinity measurement are shown in Figure 3.

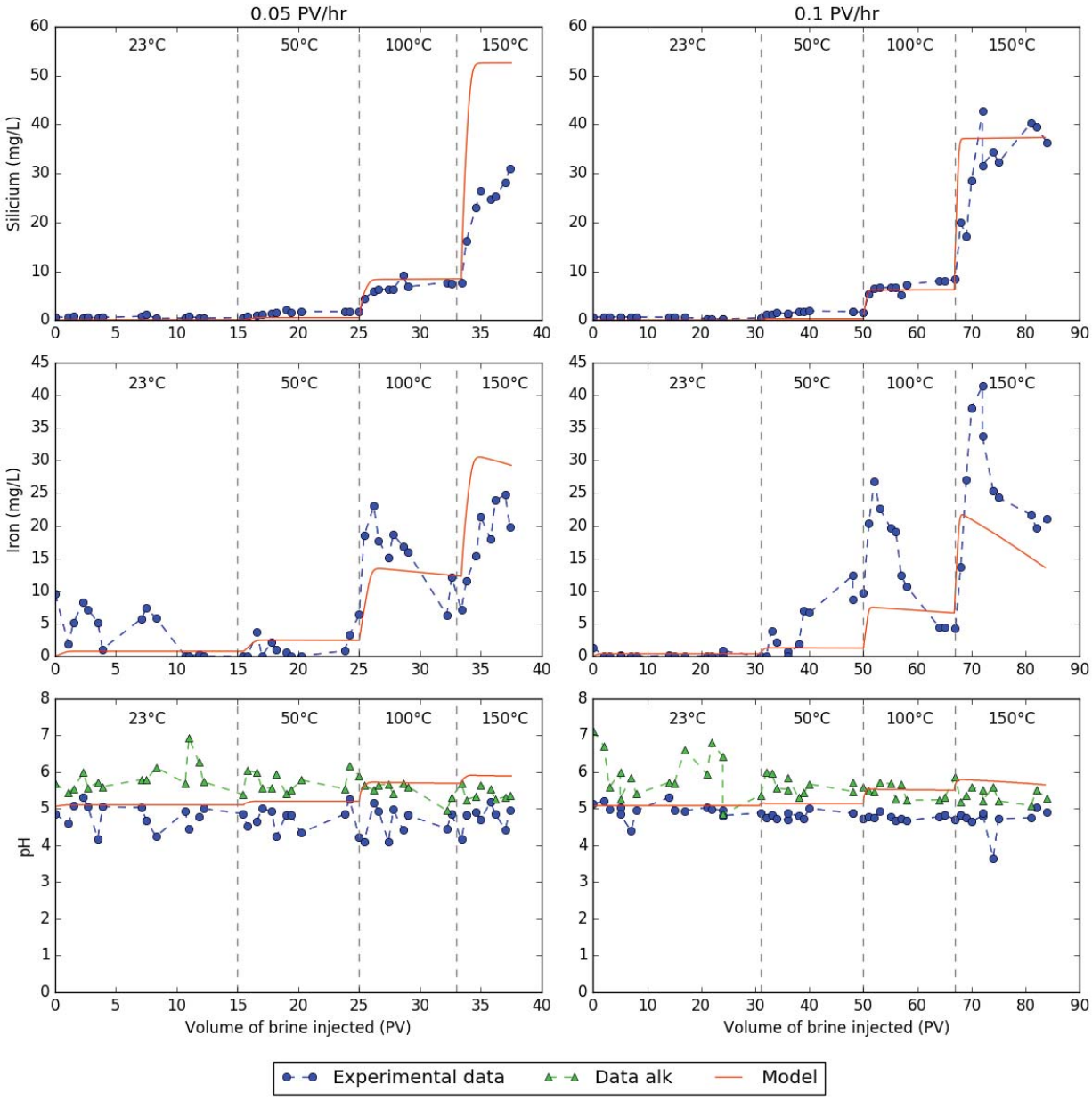

Figure 3. Measured and modelled silicium and iron concentration and pH in the effluent of a Gassum Formation column flushed with synthetic Gassum brine (Table 1) at 23°C, 50°C (reservoir temperature), 100°C and 150°C and with a flow velocity of 0.05 PV/hr (0.014 cm/hr) and 0.1 PV/hr (0.029 cm/hr). Measured data for the pH includes both the pH measurement (Experimental data) and the pH measured as the starting point in the alkalinity measurement (Data alk). The

model includes kinetically controlled dissolution/precipitation of albite, kaolinite, quartz and siderite (Table 2).

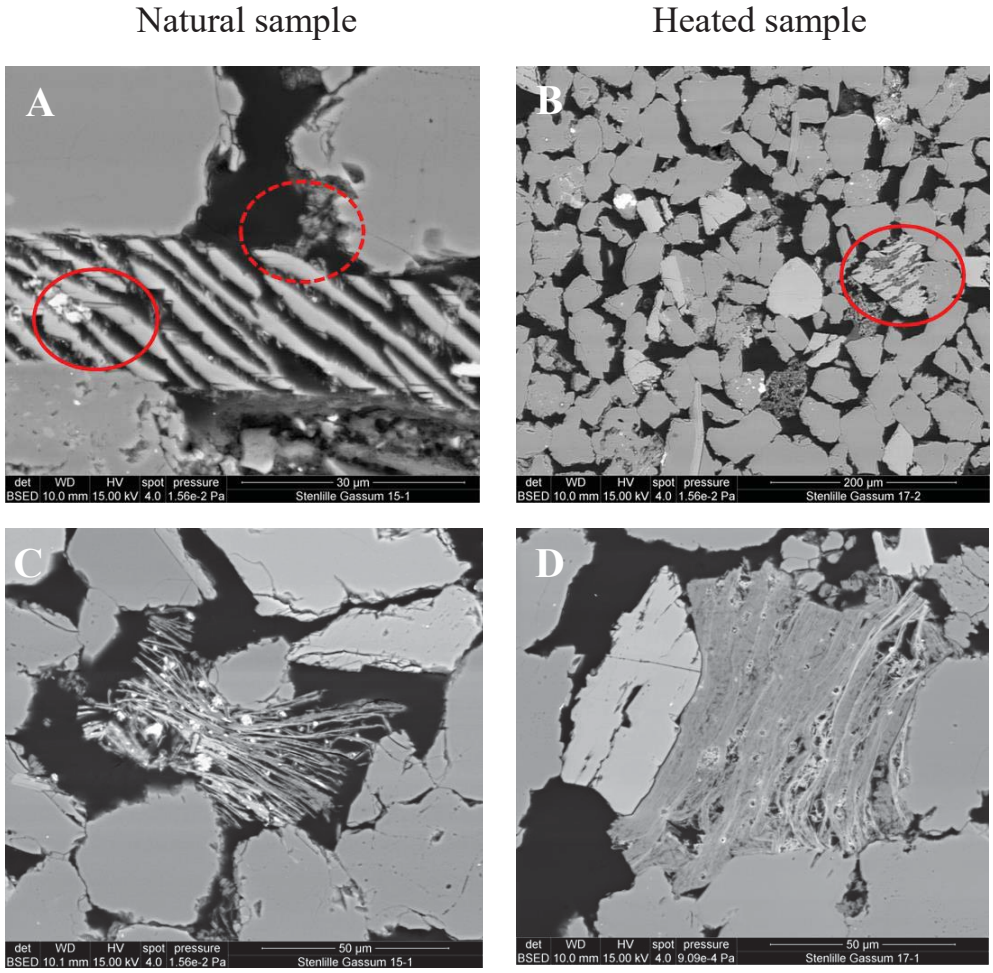

Figure 4. Petrographic analyses of the mineralogical changes due to heating of the Gassum Sandstone Formation. A: Na-rich feldspar may have been dissolved from space among K-feldspar lamella in natural sample (Circle) and kaolinite precipitated (Stippled circle) B: Kaolinite replacing albite in kali-feldspar in heated sample. C: Small crystal of siderite associated with mica in natural sample. D: Fe-poor mica displaying holes after dissolved siderite in heated sample.

3.2. Mineralogical changes. For the dominating quartz mineral, no changes were observed as a result of flooding. As previously observed in natural samples[30], the Na-rich part of exsolved alkalifeldspar is partly degraded and to some extent replaced by kaolinite. This process may well have been promoted by the flooding experiment (Figure 4A and 4C). The flooding has caused siderite to go into dissolution as evidenced by the presence of moulds after siderite crystals among mica flakes (Figure 4B and 4D).

3.3. Reactive transport modelling. Based on the observed mineralogical changes as well as the observed changes in the aqueous concentrations during the experiments, the geochemical model was fitted to the experimental data to help identify which minerals may possibly dissolve and/or precipitate when heated Gassum brine is injected into the Gassum Formation. The model optimised to the experimental data includes the minerals albite (as a proxy for Na-rich alkalifeldspar), kaolinite, quartz and siderite with kinetic parameters that are generally in accordance with the literature (Table 2).

Even though quartz dissolution was not identified by the petrographic analysis, the reaction was included in the model to reach the high silicium concentrations measured, especially at 150°C. No trace of amorphous silica phases have been identified in the Gassum Formation[27, 29]. Calcite was not detected by petrography or in previous studies in the Gassum Formation in the Stenlille area[27, 29] and therefore calcite is not included in the model. Simple speciation calculations show subsaturation with respect to calcite in the effluent brine. Since calcite dissolution would be fast compared to the residence time in the specimens, this confirms that dissolution of calcite is not likely to occur in the experiment.

Table 2. Specific surface area (SSA), initial mass of mineral (m_0) and kinetic parameters used for the reactive transport model[39].

			Acid mechanisms			Neutral mechanism		Alkali mechanism		
	SSA	m_0	log(k25)	E_a	n	log(k25)	E_a	log(k25)	E_a	n
	(m^2/g)	(g)	($mol/m^2/s$)	(kJ/mol)	(-)	($mol/m^2/s$)	(kJ/mol)	($mol/m^2/s$)	(kJ/mol)	(-)
Quartz	0.038	67.98	-	-	-	-13.99	87.7	-	-	-
Albite	0.115	0.52	-10.16	65.0	0.457	-12.56	69.8	-15.6	71.0	-0.572
Kaolinite	0.185	0.31^{+}	-11.31	65.9	0.777	-13.18	22.2	-17.05	17.9	0.472
Siderite*	$3.8 \cdot 10^{-5}$	$0.1 \cdot 10^{-2+}$	-3.19	36.1	0.500	-7.53	52.2	-5.11	34.8	0.500

*Data for siderite are assumed equivalent to dolomite[44]

$^{+}$ Adjusted in the optimized model

A strong coupling between Na-rich alkalifeldspar dissolution and kaolinite precipitation is observed as changes in the kaolinite precipitation rate affects the modelled aluminium and silicium concentrations. The rate of kaolinite precipitation is therefore constrained by both the silicium and aluminium concentrations. The best fit of the model to the measured data was obtained when applying a specific surface area for kaolinite of 0.185 m^2/g , which is very low for typical kaolinite but within the range of previously reported values[39]. For siderite, the best fit of the model to the measured iron concentrations was obtained by applying a specific surface area of $3.83*10^{-5}$ m^2/g.

Figure 3 shows the results of the geochemical model together with the experimental data for the flooding experiments. The measured silicium and iron concentration as well as the pH are predicted reasonably well for both experiments with the model optimised for the 0.1 PV/hr experiment. Furthermore, in accordance with the measured aluminium concentrations, the model predicts the aqueous aluminium concentration to be 0.01 to 0.06 mg/l and thus near the detection limit (0.03 mg/L).

3.4. Silicium. For both experiments, the model reproduces the immediate increase in the silicium concentration upon each temperature increase as well as the concentration level reached at each temperature. The exception is the significantly lower measured silicium concentration at 150°C in the 0.05 PV/hr experiment (ca. 30 mg/L) as compared to the concentration predicted by the model (52 mg/L). When sampling, the effluent from the 0.1 PV/hr experiment was always sampled first, leaving the sampling loop for the 0.05 PV/hr experiment at 23°C for approximately 30 min. As the solubility of SiO_2 minerals decreases with decreasing temperature[8, 45], it is possible that a SiO_2 mineral, probably amorphous silica, has precipitated in the vial during this period of time, resulting in a lower measured aqueous silicium concentration. Assuming the silicium concentration predicted by the model in the effluent from the experiment (52 mg/L), a simple speciation simulation with PHREEQC[32] shows that the effluent from the 0.05 PV/hr experiment at 150°C becomes slightly supersaturated with respect to amorphous silica (SI = 0.09) upon cooling to 23°C, For comparison, the effluent from the 0.1 PV/hr experiment is sub-saturated with respect to amorphous silica at both 150°C and upon cooling to 23°C (SI = -0.06). Precipitation of amorphous silica from geothermal water has been shown to be fast (within one hour) upon cooling from 250°C to 25°C[46].

Confirming the petrographic analysis, the model results show that at reservoir conditions (50°C) dissolution of Na-rich alkalifeldspar and precipitation of kaolinite occurs (Figure 5). Weathering of Na-feldspar to kaolinite can be illustrated by the following reaction:

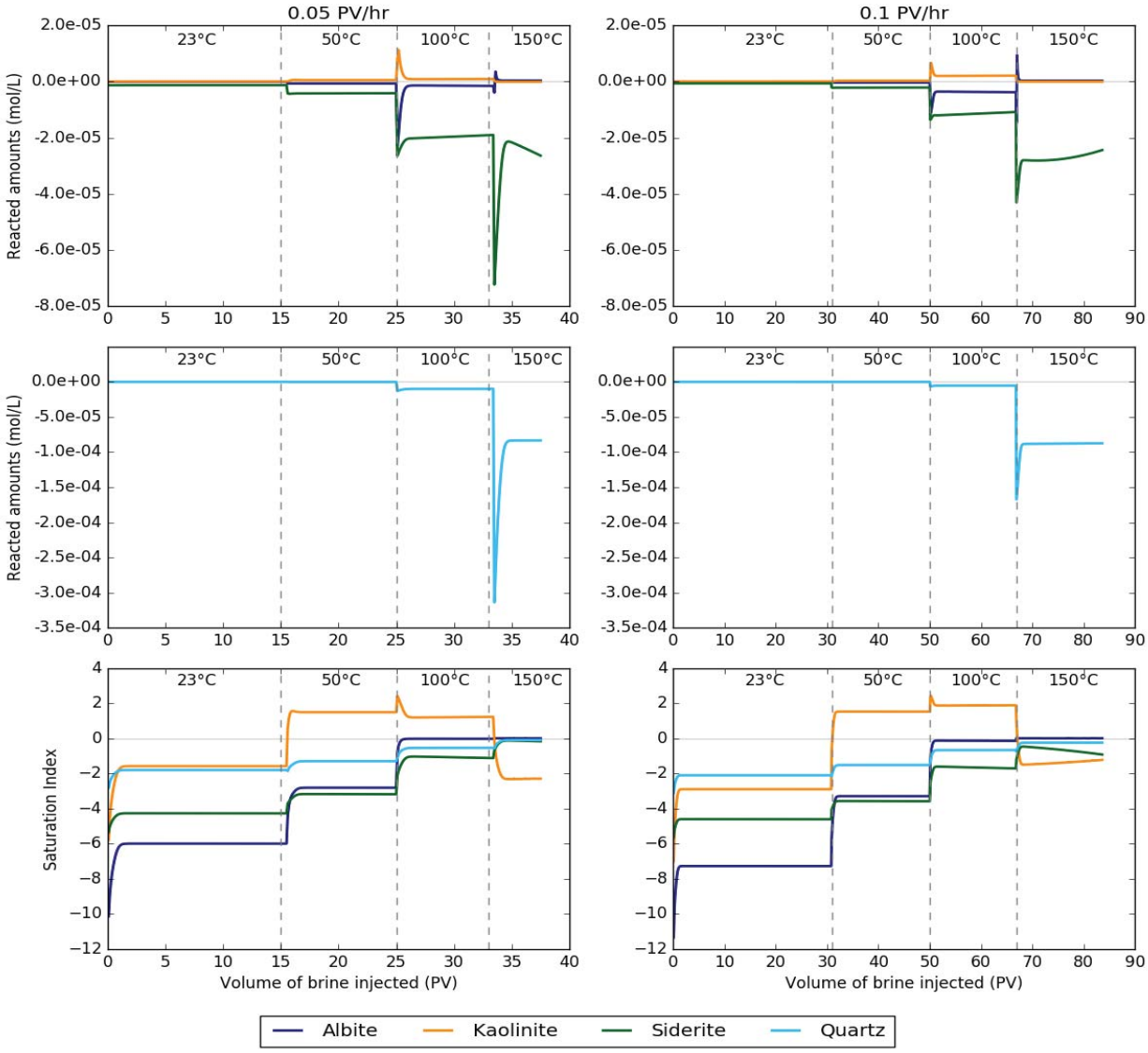

Figure 5. Reacted amounts and the Saturation Index for minerals included in a PHREEQC transport model of synthetic Gassum brine (Table 1) through a column in which kinetically controlled (Table 2) dissolution or precipitation of albite, kaolinite, siderite and quartz is allowed at 0.05 PV/hr (0.014 cm/hr) and 0.1 PV/hr (0.029 cm/hr). A positive "Reacted amounts" indicates

that the mineral precipitates, while a negative value indicates dissolution of the mineral. The saturation state of the effluent is indicated by the Saturation Index; the possibility of dissolution and precipitation revealed by a negative and positive value of the saturation index, respectively.

Feldspar Kaolinite

$$NaAlSi_3O_8 + H^+ + 0.5H_2O \rightarrow 0.5Al_2Si_2O_5(OH)_4 + Na^+ + 2SiO_{2(aq)}$$

Upon a temperature increase to 100°C, the conversion of feldspar to kaolinite is expected to increase (Figure 5) due to a higher rate of dissolution of feldspar and precipitation of kaolinite with increasing temperature[9, 10, 47]. With increasing temperature, the solution approaches saturation with respect to albite (Figure 5). Equilibrium is, however, not reached even at 100°C where the simulated saturation indices for albite are -0.66 and -0.02 for the 0.1 PV/hr and 0.05 PV/hr experiment, respectively. The generally negative saturation indices simulated for temperatures ≤100°C indicate that the aqueous silicium concentration is not controlled by equilibrium with either of the silicium containing mineral phases. The close to constant aqueous silicium concentration measured irrespective of the flow velocity (Figure 3) suggests that the silicium concentration is controlled by a quasi-stationary state between feldspar dissolution and kaolinite precipitation. The flow rate affects the magnitude of the dissolution/precipitation processes in this quasi-stationary state. Thus, at 100°C more feldspar is dissolved and kaolinite precipitated at the higher flow as compared to the lower flow rate due to a lower saturation index in the first case. These contra-intuitive results are in line with previous observations by Zhu et al., (2010)[48] who found that a quasi-steady state determined by the relative rate of albite dissolution and precipitation of secondary minerals was reached. In line with our results a strong coupling between dissolution, precipitation and flow rates was observed. Thus depending on the flow rate, the quasi steady-state was reached at different levels of saturation index[48].

With increasing temperature, dissolution of quartz becomes increasingly important, and at 100°C the dissolution of quartz is in the same order of magnitude as the dissolution of Na-richfeldspar. However, at 150°C the dissolution of quartz increases sharply resulting in a significant increase in the aqueous silicium concentration (Figure 3). Thus, at 150°C quartz dissolution becomes the predominant process, completely suppressing the dissolution of feldspar and thereby the precipitation of kaolinite (Figure 5). At 150°C, the silicium concentration is solely controlled by the dissolution kinetics of quartz and therefore a higher silicium concentration is predicted by the model at 150°C at the velocity of 0.05 PV/hr as compared to 0.1 PV/hr.

3.5. Iron. The petrographic analysis clearly shows that dissolution of siderite occurs during the flooding experiments (Figure 4). Figure 3 shows that the model reproduces the immediate increase in the iron concentration upon a temperature increase followed by a decrease in the iron concentration. According to the model, the decreasing iron concentration is a consequence of a decrease in the siderite content as the dissolution progresses. Particularly for the 0.1 PV/hr experiment, the model, however, underestimates the iron concentration. Thus, dissolution of siderite may not account for all of the iron released to solution during the core flooding experiments. Tests including biotite in the model do not increase the iron concentration significantly. Release of iron due to corrosion of the equipment is unlikely since high corrosion-resistant Hastelloy®(C-276) was used in the experimental setup. Moreover a concomitant release by other elements present in the Hastelloy® in significant amounts (Ni, Cr, Mo, W, Co) was not observed.

4. CONCLUSION

Core flooding experiments, petrographic analysis and geochemical modelling of the chemical effects of heat storage of up to 150°C in the Gassum Sandstone Formation in the Stenlille area

show that the heating of the reservoir is expected to enhance the naturally occurring weathering of Na-rich feldspar to kaolinite and induce dissolution of quartz and siderite. Assuming a constant dissolution rate in the entire storage period, extrapolation of the model results indicates that less than 0.05% and 0.6% of the quartz in the reservoir will dissolve during storage at 100°C or 150°C, respectively, for six months and thus quartz dissolution is not expected to significantly deteriorate the reservoir properties. Likewise, up to 3.2% of the Na-rich feldspar present in the reservoir will dissolve during a six month storage at 100°C. Due to the small content of feldspar present in the reservoir this is not expected to reduce the mechanical strength of the reservoir. The formation of kaolinite will, however, increase the formation damaging potential of the reservoir as the presence of even small amounts of kaolinite is known to potentially decrease the reservoir permeability under certain conditions. Thus, the decline in permeability commonly observed due to heating is often explained with mobilisation of colloidal particles e.g. kaolinite[49-51]. No measureable changes are, however, observed in the porosity and permeability of the tested specimens before and after the experiments, indicating no formation damage of the specimens due to the flooding of heated formation water (Table 3). In line with this, permeability tests with specimens from Gassum Formation in the Stenlille area using synthetic brine at temperatures up to 150°C showed a small permeability increase due to heating[11].

Major changes observed in the brine composition include increased silicium and iron content caused by the heating induced dissolution processes. To ensure sustainable energy production from the heat storage, appropriate removal of these elements e.g. by filtration in the surface facility is consequently critical to prevent clogging of the injection well due to re-precipitation of silicium and iron upon cooling of the brine. As the aqueous concentration of both silicium and iron increases sharply above 100°C, keeping the storage temperature below 100°C, as observed at other

heat storage facilities[52], may help reduce the chemical effects of the heat storage on the reservoir and thereby any injection problems.

Table 3. Measured porosity and gas permeability of the tested samples before and after the flooding experiments.

		Pre experiment		Post experiment	
Sample	Flow rate (PV/hr)	Porosity (%)	Permeability mD	Porosity (%)	Permeability mD
$S_{0.05}$	0.05	29.11 ± 0.1	195 ± 10	29.04 ± 0.1	181 ± 9
$S_{0.1}$	0.1	28.85 ± 0.1	181 ± 9	28.77 ± 0.1	n.a*

*As a small part of the $S_{0.1}$ sample broke off during the dismantling of the sample from the core holder it was not possible to measure the permeability after the experiment.

In conclusion, the results of this study show that the chemically induced effects of heat storage in the Gassum Formation in the Stenlille area may be of minor importance and that heat storage in the Gassum Formation in the Stenlille area may be possible provided operational precautions are taken.

AUTHOR INFORMATION

Corresponding Author

*e-mail: hdh@geus.dk.

ACKNOWLEDGMENT

This research was funded by the Danish Council for Strategic Research (now Innovation Fund Denmark) as part of the Heat Storage in Hot Aquifers (HeHo) project (Grant 10-093934). We thank Rikke Weibel at GEUS for help with the description of the Gassum Formation and three anonymous reviewers for their comments.

REFERENCES

(1) Lund, J. W.; Freeston, D. H.; Boyd, T. L., Direct utilization of geothermal energy 2010 worldwide review. *Geothermics* **2011,** *40*, (3), 159-180. DOI: 10.1016/j.geothermics.2011.07.004.

(2) Kabus, F.; Hofmann, F.; Möllmann, G. In *Aquifer storage of waste heat arising from a gas and steam cogeneration plant - concept and first operating experience*, World Geothermal Congress 2005, Antalya, Turkey, 24-29 April 2005.

(3) Réveillère, A.; Hamm, V.; Lesueur, H.; Cordier, E.; Goblet, P., Geothermal contribution to the energy mix of a heating network when using Aquifer Thermal Energy Storage: Modeling and application to the Paris basin. *Geothermics* **2013,** *47*, 69-79. DOI: 10.1016/j.geothermics.2013.02.005.

(4) Appelo, C. A. J.; Postma, D., *Geochemistry, groundwater and pollution*. 2nd ed.; A. A. Balkema Publisher: 2005.

(5) Brons, H. J.; Griffioen, J.; Appelo, C. A. J.; Zehnder, A. J. B., (Bio)geochemical reactions in aquifer material from a thermal-energy storage site. *Water Res.* **1991,** *25*, (6), 729-736. DOI: 10.1016/0043-1354(91)90048-u.

(6) Griffioen, J.; Appelo, C. A. J., Nature and extent of carbonate precipitation during aquifer thermal-energy storage. *Appl. Geochem.* **1993,** *8*, (2), 161-176. DOI: 10.1016/0883-2927(93)90032-c.

(7) Hoyer, M.; Hallgren, J.; Eisenreich, S.; Sterling, R., Field-test results of aquifer thermal energy storage at St. Paul, Minnesota. *J. Energy Eng.* **1994,** *120*, (2), 67-85. DOI: 10.1061/(ASCE)0733-9402(1994)120:2(67).

(8) Dove, P. M.; Crerar, D. A., Kinetics of quartz dissolution in electrolyte solutions using a hydrothermal mixed flow reactor. *Geochim. Cosmochim. Acta* **1990,** *54*, (4), 955-969. DOI: 10.1016/0016-7037(90)90431-J.

(9) Gruber, C.; Kutuzov, I.; Ganor, J., The combined effect of temperature and pH on albite dissolution rate under far-from-equilibrium conditions. *Geochim. Cosmochim. Acta* **2016,** *186*, 154-167. DOI: 10.1016/j.gca.2016.04.046.

(10) Palandri, J. L.; Kharaha, Y. K. *A compilation of rate parameters of water-mineral interaction kinetics for application to geochemical modeling*; U.S. Geological Survey Water-Resources Investigations Report 04-1068, 2004.

(11) Holmslykke, H. D.; Kjøller, C.; Fabricius, I. L., The effect of heating and flow velocity on the permeability in the Gassum and Bunter Sandstone Formations. **In prep**.

(12) Tenthorey, E.; Scholz, C. H.; Aharonov, E.; Leger, A., Precipitation sealing and diagenesis - 1. Experimental results. *J. Geophys. Res.: Solid Earth* **1998,** *103*, (B10), 23951-23967. DOI: 10.1029/98jb02229.

(13) Moore, D. E.; Morrow, C. A.; Byerlee, J. D., Chemical reactions accompanying fluid flow through granite held in a temperature gradient. *Geochim. Cosmochim. Acta* **1983,** *47*, (3), 445-453. DOI: 10.1016/0016-7037(83)90267-3.

(14) Bonte, M.; Stuyfzand, P. J.; van Breukelen, B. M., Reactive transport modeling of thermal column experiments to investigate the impacts of aquifer thermal energy storage on groundwater quality. *Environ. Sci. Technol.* **2014,** *48*, (20), 12099-12107. DOI: 10.1021/es502477m.

(15) Possemiers, M.; Huysmans, M.; Batelaan, O., Influence of aquifer thermal energy storage on groundwater quality: A review illustrated by seven case studies from Belgium. *J. Hydrol. Reg. Stud.* **2014,** *2*, 20-34. DOI: 10.1016/j.ejrh.2014.08.001.

(16) Perlinger, J. A.; Almendinger, J. E.; Urban, N. R.; Eisenreich, S. J., Groundwater geochemistry of aquifer thermal energy storage - Long term test cycle. *Water Resour. Res.* **1987,** *23*, (12), 2215-2226. DOI: 10.1029/WR023i012p02215.

(17) Vetter, A.; Mangelsdorf, K.; Schettler, G.; Seibt, A.; Wolfgramm, M.; Rauppach, K.; Vieth-Hillebrand, A., Fluid chemistry and impact of different operating modes on microbial community at Neubrandenburg heat storage (Northeast German Basin). *Org. Geochem.* **2012,** *53*, 8-15. DOI: 10.1016/j.orggeochem.2012.08.008.

(18) Holmslykke, H. D.; Kjøller, C.; Fabricius, I. L., Core flooding experiments and reactive transport modelling of heat storage in the Bunter Sandstone Formation. **In prep**.

(19) Azaroual, M.; Fouillac, C., Experimental study and modelling of granite-distilled water interactions at 180 degrees C and 14 bars. *Appl. Geochem.* **1997,** *12*, (1), 55-73. DOI: 10.1016/s0883-2927(96)00054-6.

(20) Schepers, A.; Milsch, H., Dissolution-precipitation reactions in hydrothermal experiments with quartz-feldspar aggregates. *Contrib. Mineral. Petrol.* **2013,** *165*, (1), 83-101. DOI: 10.1007/s00410-012-0793-x.

(21) Gong, Q.; Deng, J.; Han, M.; Yang, L.; Wang, W., Dissolution of sandstone powders in deionised water over the range 50–350 °C. *Appl. Geochem.* **2012,** *27*, (12), 2463-2475. DOI: 10.1016/j.apgeochem.2012.08.011.

(22) Fu, Q.; Lu, P.; Konishi, H.; Dilmore, R.; Xu, H.; Seyfried Jr, W. E.; Zhu, C., Coupled alkali-feldspar dissolution and secondary mineral precipitation in batch systems: 1. New experiments at 200 °C and 300 bars. *Chem. Geol.* **2009,** *258*, (3–4), 125-135. DOI: 10.1016/j.chemgeo.2008.09.014.

(23) Nielsen, L. H., Late Triassic-Jurassic development of the Danish Basin and the Fennoscandian Border Zone, southern Scandinavia. In *The Jurassic of Denmark and Greenland*, Ineson, J. R.; Surlyk, F., Eds. Geological Survey of Denmark and Greenland Bulletin 1, 2003; pp 459-526.

(24) Nielsen, L. H.; Japsen, P. *Deep wells in Denmark 1935-1990. Lithostratigraphic subdivision*; Geological Survey of Denmark A 31, 1991; p 179 pp.

(25) Laier, T.; Øbro, H., Environmental and safety monitoring of the natural gas underground storage at Stenlille, Denmark. In *Underground gas storage: Worldwide experiences and future development in the UK and Europe.*, Evans, D. J.; Chadwick, R. A., Eds. The Geological Society, London, Special Publication, 2009; Vol. 313, pp 81-92.

(26) Liboriussen, J.; Ashton, P.; Thygesen, T., The tectonic evolution of the Fennoscandian Border Zone in Denmark. In *Compressional intraplate deformations in the Alpine Foreland*, Ziegler, P. A., Ed. Tectonophysics, 1987; Vol. 137, pp 21-29.

(27) Friis, H. *Diagenesis of the Gassum Formation Rhaetian-Lower Jurassic, Danish Subbasin*; Geological Survey of Denmark A 18: 1987; p 41pp.

(28) McBride, E. F., A classification of common sandstones. *J. Sediment. Petrol.* **1963,** *33*, 664-669.

(29) Weibel, R.; Olivarius, M.; Kristensen, L.; Friis, H.; Hjuler, M. L.; Kjøller, C.; Mathiesen, A.; Nielsen, L. H., Predicting permeability of low-enthalpy geothermal reservoirs: A case study from the Upper Triassic – Lower Jurassic Gassum Formation, Norwegian–Danish Basin. *Geothermics* **2017,** *65*, 135-157. DOI: 10.1016/j.geothermics.2016.09.003.

(30) Weibel, R.; Olivarius, M.; Nielsen, L. H.; Abramovitz, T.; Kjoller, C. *Petrography and diagenesis of the Triassic and Jurassic sandstones, eastern part of the Norwegian-Danish Basin*; Geological Survey of Denmark and Greenland report 114: 2010; p 88pp.

(31) Laier, T. *Chemistry of Danish saline formation waters relevant for core fluid experiments – Fluid chemistry data for lab experiments related to CO_2 storage on deep aquifers*; GEUS report 2008/48: 2008.

(32) Parkhurst, D. L.; Appelo, C. A. J., *Description of input and examples for PHREEQC version 3 - A computer program for speciation, batch-reaction, one-dimensional transport, and inverse geochemical calculations*. U.S. Geological Survey Techniques and Methods, 2013; Vol. book 5, chap. A43, 497 p. Available only at http://pubs.usgs.gov/tm/06/a43/.

(33) Blanc, P.; Lassin, A.; Piantone, P. Thermodem: A database devoted to waste minerals. http://thermoddem.brgm.fr/

(34) API, *Recommended practice for core analysis - Recommended practice 40, second edition*. American Petroleum Institute: Washington DC, 1998; p 236.

(35) Stumm, W.; Morgan, J. J., *Aquatic Chemistry*. John Wiley, N. Y., 1981.

(36) Atkins, P. W.; de Paula, J., *Atkins' physical chemistry*. 7th ed.; oxford Univ. Press, 2002.

(37) Pitzer, K. S., Characteristics of very concentrated aqueous solutions. *Physics and Chemistry of the Earth* **1981,** *13*, 249-272. DOI: 10.1016/0079-1946(81)90013-6.

(38) Plummer, L. N.; Parkhurst, D. L.; Fleming, G. W.; Dunkle, S. A. *A computer program incorporating Pitzer's equations for calculation of geochemical reactions in brines*; 88-4153; 1988.

(39) Cantucci, B.; Montegrossi, G.; Vaselli, O.; Tassi, F.; Quattrocchi, F.; Perkins, E. H., Geochemical modeling of CO_2 storage in deep reservoirs: The Weyburn Project (Canada) case study. *Chem. Geol.* **2009,** *265*, (1–2), 181-197. DOI: 10.1016/j.chemgeo.2008.12.029.

(40) André, L.; Audigane, P.; Azaroual, M.; Menjoz, A., Numerical modeling of fluid–rock chemical interactions at the supercritical CO_2–liquid interface during CO_2 injection into a carbonate reservoir, the Dogger aquifer (Paris Basin, France). *Energy Convers. Manage.* **2007,** *48*, (6), 1782-1797. DOI: 10.1016/j.enconman.2007.01.006.

(41) Chou, L.; Wollast, R., Study of the weathering of albite at room-temperature and pressure with a fluidized-bed reactor. *Geochim. Cosmochim. Acta* **1984,** *48*, (11), 2205-2217. DOI: 10.1016/0016-7037(84)90217-5.

(42) Berner, R. A.; Holdren, G. R., Mechanism of feldspar weathering 2. Observations of feldspars from soils. *Geochim. Cosmochim. Acta* **1979,** *43*, (8), 1173-1186. DOI: 10.1016/0016-7037(79)90110-8.

(43) Holdren, G. R.; Speyer, P. M., Reaction rate-surface area relationships during the early stages of weathering 1. Initial observations. *Geochim. Cosmochim. Acta* **1985,** *49*, (3), 675-681. DOI: 10.1016/0016-7037(85)90162-0.

(44) Gunter, W. D.; Perkins, E. H.; Hutcheon, I., Aquifer disposal of acid gases: modelling of water–rock reactions for trapping of acid wastes. *Appl. Geochem.* **2000,** *15*, (8), 1085-1095. DOI: 10.1016/S0883-2927(99)00111-0.

(45) Rimstidt, J. D.; Barnes, H. L., The kinetics of silica-water reactions. *Geochim. Cosmochim. Acta* **1980,** *44*, (11), 1683-1699. DOI: 10.1016/0016-7037(80)90220-3.

(46) Dixit, C.; Bernard, M.-L.; Sanjuan, B.; André, L.; Gaspard, S., Experimental study on the kinetics of silica polymerization during cooling of the Bouillante geothermal fluid (Guadeloupe, French West Indies). *Chem. Geol.* **2016,** *442*, 97-112. DOI: 10.1016/j.chemgeo.2016.08.031.

(47) Manning, D. A. C., Experimental studies of clay mineral occurrence. In *Clay mineral cements in sandstones (Special publication number 34 of the international association of sedimentologists)*, Worden, R. H.; Morad, S., Eds. Blackwell publishing: 2003; pp 177-190.

(48) Zhu, C.; Lu, P.; Zheng, Z.; Ganor, J., Coupled alkali feldspar dissolution and secondary mineral precipitation in batch systems: 4. Numerical modeling of kinetic reaction paths. *Geochim. Cosmochim. Acta* **2010,** *74*, (14), 3963-3983. DOI: 10.1016/j.gca.2010.04.012.

(49) Rosenbrand, E.; Haugwitz, C.; Jacobsen, P. S. M.; Kjoller, C.; Fabricius, I. L., The effect of hot water injection on sandstone permeability. *Geothermics* **2014,** *50*, 155-166. DOI: 10.1016/j.geothermics.2013.09.006.

(50) Rosenbrand, E.; Kjoller, C.; Riis, J. F.; Kets, F.; Fabricius, I. L., Different effects of temperature and salinity on permeability reduction by fines migration in Berea sandstone. *Geothermics* **2015,** *53*, 225-235. DOI: 10.1016/j.geothermics.2014.06.004.

(51) Schembre, J. M.; Kovscek, A. R., Mechanism of formation damage at elevated temperature. *J. Energy Resour. Technol. Trans. ASME* **2005,** *127*, (3), 171-180. DOI: 10.1115/1.1924398.

(52) Kabus, F.; Wolfgramm, M. In *Aquifer thermal energy storage in Neubrandenburg-monitoring throughout three years of regular operation*, Proceedings of the 11th international conference on energy storage 2009, Stockholm, Sweden, 2009; p 8pp.

For table of contents only